Ecole Publique d'Ingénieurs en 3 ans

Report

Fiber induced optical phase noise cancellation

Presentation date : 22/08/2024

Engineering Internship 2nd year – 2023/2024

Camille Perinet
Academic year 2023/2024
Electronics and Applied Physics Maj. Physical Engineering and Sensors

EGO Supervisor : Camilla DE ROSSI
ENSICAEN Supervisor : Hervé GILLES

CONTENTS

1. Introduction **4**

1.1. EGO VIRGO and the Optic Group 4

1.2. Presentation of the subject 5

2. Background and state of the art **5**

2.1. Recommission of the second harmonic generation setup 5

2.2. Theory of optical phase noise and phase modulation 8

2.3. Theory of the beating 10

2.4. Working principal of utilized components 13

2.4.1. Mirror on a tip / tilt platform 13

2.4.2. Fiber stretcher 14

3. Phase noise cancellation experimental setup **15**

3.1. General overview of the setup 15

3.2. Modulation and demodulation 16

3.3. Beating measurements 17

4. Feedback loop **19**

4.1. General overview 19

4.2. Open loop transfer function 20

4.3. Results and optimization 21

5. Conclusion and perspectives **22**

Acknowledgements

I would like to express my sincere gratitude to all those who have supported and guided me throughout my internship and the preparation of this report.

My thanks go first of all to Camilla De Rossi for the quality of her supervision and for the time and effort she dedicated to me all along this internship.

I also would like to express my gratitude to Matthieu Gosselin, Julia Casanueva, Maddalena Mantovani and Piernicola Spinicelli for their help on this project.

I extend my thanks to all the members of Virgo for their kindness, inclusion, and welcoming spirit, which made my experience truly memorable.

1. Introduction

1.1. EGO VIRGO and the Optic Group

The Virgo interferometer, the most sensitive gravitational-wave detector in Europe, operates by using laser beams to measure tiny distortions in space-time caused by the passage of gravitational waves. It was initially realized through a partnership between the French and Italian institutes CNRS and INFN, then joined by the Dutch National Institute for Nuclear and High energy physics (NIKHEF). Nowadays, 142 institutions in 16 different countries are part of the Virgo collaboration. The Virgo experiment is hosted by the European Gravitational Observatory (EGO) consortium in the countryside near Pisa in Italie. EGO's organization is composed of several groups assuring the correct operation of the detector, upgrades and research directly related on the detector. The Optic group, which I joined for my internship, is responsible for the injection system (INJ) and plays a major role in the Auxiliary Laser System (ALS).

The detection principle of Virgo is based on a Michelson interferometer configuration (figure 1). A laser beam is split into two long arms of 3 km each by a beam splitter. The two beams are reflected by mirrors at the end of each arm back to the beam splitter, where they recombine. To increase the signal the two input and end mirrors in each arm form two Fabry-Perot cavities. The Power Recycling mirror as well as the Signal Recycling mirror form also two other recycling cavities. In the end the laser path is folded hundreds of times before the light recombines at the beam splitter, amplifying the gravitational wave signal by about a factor 300. At the beamsplitter, the two beams interfere with each other, the interference pattern depends on the difference in the travel time of the beams along the two arms. When no gravitational waves interfere with the interferometer the pattern is a dark fringe, the beams recombine in anti-phase. When a gravitational wave passes it causes a minuscule change in the optical path of one arm relative to the other so that the two beams are no longer in anti-phase and photons can be detected by a photodiode.[1]

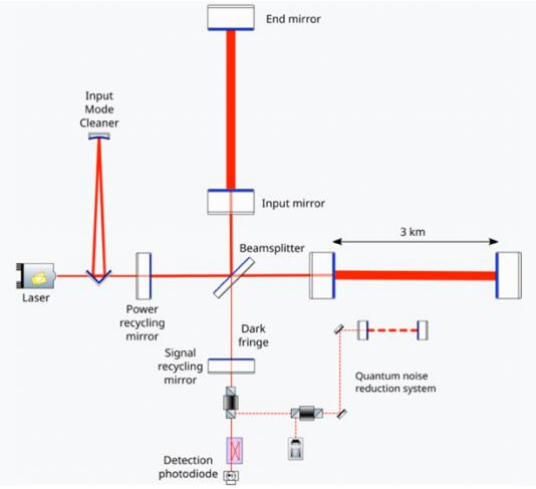

Figure 1: The optical layout of Advanced Virgo, with dual recycling and Quantum Noise Reduction (Frequency Dependent Squeezing scheme).

Following the successful observation run of 2017, the interferometer underwent significant upgrades to become « Advanced Virgo » and then « Advanced Virgo + ». This new version features improved mirrors, higher laser power, and signal recycling techniques, aiming to increase sensitivity by an order of magnitude.

1.2. Presentation of the subject

A significant upgrade in Advanced Virgo + is the installation of the signal recycling mirror, creating a new cavity known as the Signal Recycling cavity. This addition complicates the lock acquisition process for the entire interferometer. To address this, the Auxiliary Laser System has been implemented. This system uses a 532nm beam, obtained by doubling in frequency the main Virgo laser. Notably, optical fibers are utilized to propagate the beam across different points on the site, offering advantages in terms of ease of propagation, handling, and maintenance. However, a drawback is the susceptibility to environmental noise (acoustic and seismic) coupling with these fibers, introducing additional phase noise to the signals of interest.

The purpose of this internship is to build an optical set-up, electronic hardware, and a lock-scheme to accurately cancel optical phase noise induced by an optical fiber, using a piezoelectric and a fiber stretcher as actuators. In this context, the Second Harmonic Generation optical setup will be recommissioned to generate a green beam. This green beam will be the input of a second setup that will be establish in this project. The second setup is an interferometer that will be capable of measuring optical phase noise, with the focus on developing an active feedback loop to cancel it.

2. Background and state of the art

2.1. Recommission of the second harmonic generation setup

At VIRGO, the ALS uses a 532 nm laser produced by doubling in frequency the main infrared beam. The green beam is then transmitted to different buildings through optical fiber. For this reason, to build the optical setup we started by producing a green beam, which is used as an input for the phase noise cancellation setup. A second harmonic generation (SHG) setup were already built in a previous internship [2] but needed to be recommissioned. To match the characteristics of the ALS beam, we're looking to obtain a green beam of at least 50mW from a Nd-YAG 1064nm laser of 2W.

The SHG setup consist of a 1064nm beam amplified to 2W. Since the laser's polarization is not perfectly linear, it first passes through a half wave plate and two PBS to ensure an s-polarization to maximize the power of beam being reflected by high reflexive's mirrors. The lenses L1 and L2 form a telescope to obtain the correct waist in the crystal and the lens L3 collimates the beam. The infrared beam enters a nonlinear crystal where the second harmonic is generated. A dichroic mirror M3 reflects the green beam only which is then inject in the output fiber (figure 2 and 3).

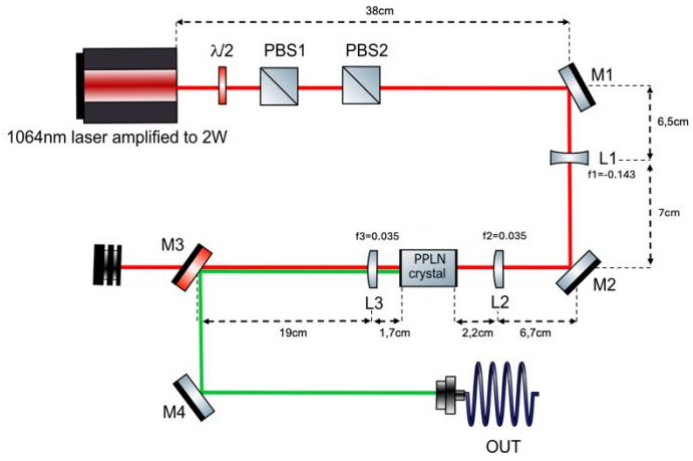

Figure 2: Schematic of the SHG setup

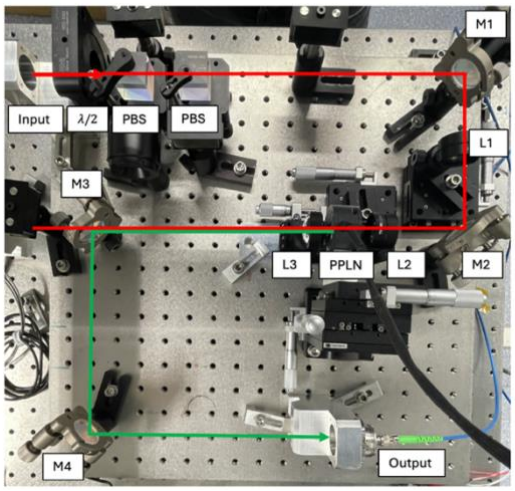

Figure 3: Image of the SHG setup

To realize a 532 nm laser source, a non-linear crystal which is a MgO-PPLN (periodically poled magnesium doped lithium niobate) crystal was used. By passing through this crystal the input laser generates a wave both the same frequency and twice the optical frequency (half the wavelength). Two inputs photons with the same wavelength of 1064 nm are combined through a nonlinear process to generate a third photon at 532 nm. The crystal is also phase matched so that the newly generated photons interfere constructively with the previously generated photons. To create constructive interferences, portions of the crystal yield are periodically inverted (poled). The poling periods depends on the input and generated beam wavelengths and the temperature of the crystal (figure 4). Our crystal contains five poled gratings with a thickness of 6.83 μm to 6.96 μm.

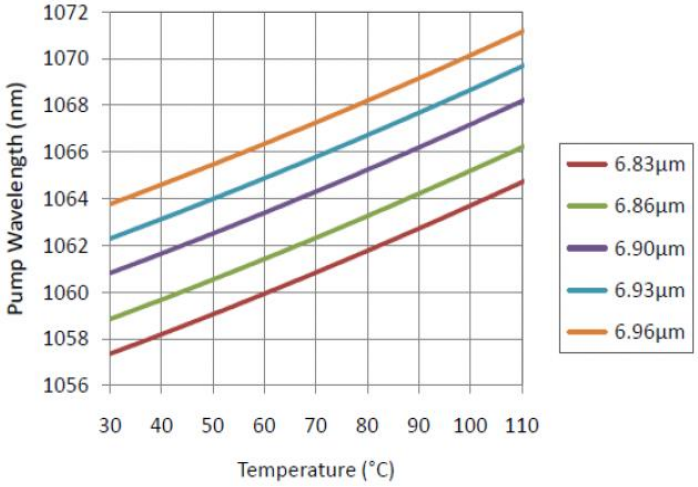

Figure 5: Relation between the periodically poled crystal, its temperature and the wavelength of the input beam

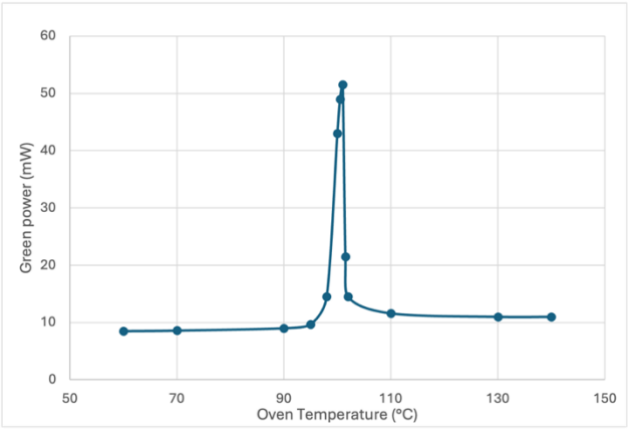

Figure 4: Measurements of the green power generated by the PPLN crystal over the oven's temperature

In the setup, the fifth grating of 6.83 μm is chosen. Differents measurements of the green power produced shows an optimal temperature of 101° (figure 5) which corresponds to the theorical value. To maintain the crystal at this constant temperature, the crystal is placed in a temperature-controlled oven.

The conversion efficiency of the SHG also depends on the waist size in the crystal which should be of 20 μm . A third lenses is used to obtain a 1.8mm collimated beam to inject in an output fiber. Various setup components had to be repositioned to obtain the correct beam width in the crystal and at the output. A telescope can be calculated (figure 7) thanks to a MATLAB program (annex 1) that gives the positions of lenses knowing their focal and the width measurements of the beam without the telescope at different positions (figure 6).

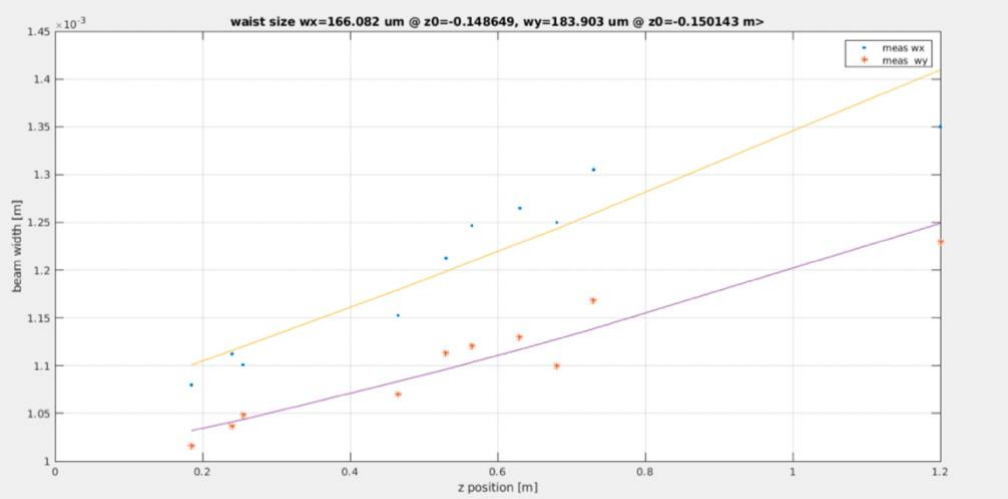

Figure 6: Fitted waist size from the different width measurements without the telescope

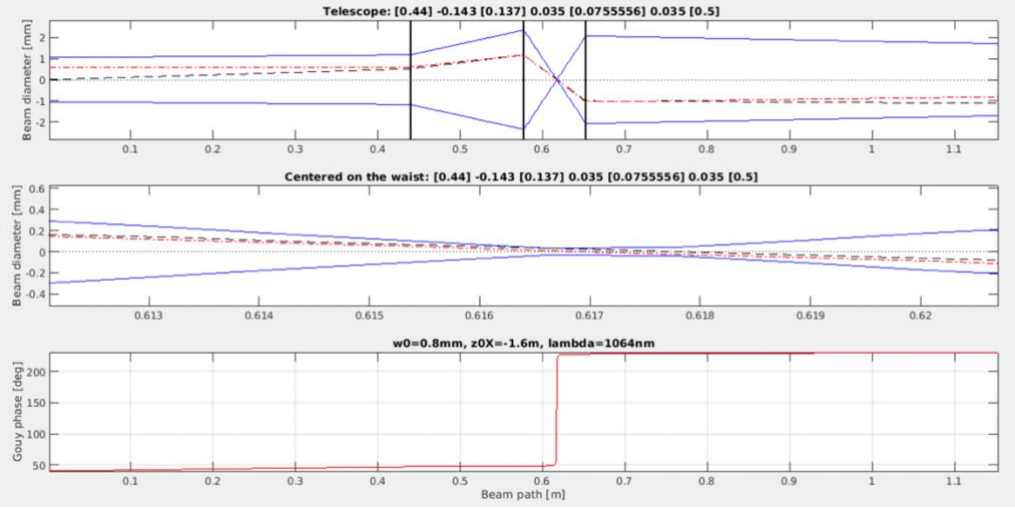

Figure 7: Simulation of the lens's positions of the telescope and beam propagation

With some millimeters differences from the results of the MATLAB program, we find experimentally the positions of the lenses as described in figure 2.

At low pump intensities, the second-harmonic conversion efficiency is small and grows linearly with increasing pump intensity, leading to a second-harmonic wave intensity proportional to the square of the pump intensity [3]: $\eta = \frac{P_{green}}{P_{seed}^2}$.

In conclusion, we measure a green power after the crystal of 50mW for the input pumped to 2W. This represents a conversion efficiency of 1.25%. The coupling of the fiber efficiency is 40%, we obtain 20mW of green power which will be the input for the noise cancellation setup.

2.2. Theory of optical phase noise and phase modulation

Phase noise in optics refers to fluctuations in the optical phase, causing the laser beam to have a broader linewidth instead of being perfectly monochromatic. This phenomenon can come from quantum noise, particularly spontaneous emission and optical losses in the gain medium, as well as environmental disturbances like temperature fluctuations affecting optical components, and mechanical vibrations of the fiber affecting the stability of the optical path. In this project, it is the vibrations due to acoustic and seismic noise that will be analyzed with the aim of cancelling it. [4]

To better localize the phase noise and create an error signal for the feedback loop to cancel the noise, we modulate the signal in phase. Therefore, in our setup, the phase noise will be added to a phase modulated signal. To better understand the resulting signal, we can in a first step described a phase modulated signal without phase noise and in a next part described the signal that contains the phase noise.

In a phase modulated signal, the phase of the carrier signal is shifted according to the modulating signal. The amplitude and frequency of the carrier signal remain constant while the amplitude of the modulating signal vary. Using a simple example of a sinusoidal phase modulation, the modulated signal can be described mathematically as follows:

$$E_{PM} = A_0\, cos(\omega_0 t + m\, cos(w_m t)) \;=\; Re(\, A_0 e^{i(\omega_0 t + m\, cos(w_m t))})$$

where

A_0 is the amplitude of the unmodulated signal and ω_0 its angular frequency.

m is the modulation index which corresponds to the maximum difference between the phase of the modulated oscillator and the unmodulated one.

w_m is the modulation frequency.

A phase-modulated signal cannot be represented by a single frequency due to the variation in phase. Instead, its frequency spectrum consists of a series of frequency components. The complexity of the spectrum depends on the modulation index m and the modulation frequency w_m.

The modulation term of the exponential $e^{(im\,cos(w_m t))}$ can be developed with the Jacobi-Anger expansion [5]:

$$e^{(im\cos(w_m t))} = J_0(m) + 2\sum_{n=1}^{\infty} i^n J_n(m)\cos(n\,w_m t)$$

$$= J_0(m) + 2i\,J_1(m)\cos(w_m t) + 2i^2 J_2(m)\cos(2w_m t) + \cdots + 2i^n J_n(m)\cos(n\,w_m t) + \cdots$$

Where J is the Bessel function of the first kind.

The phase modulated signal can now be developed:

$$E_{PM} = A_0 \times (\, J_0(m)e^{iw_0 t} + i\,J_1(m)\left[\, e^{i(w_0 t + w_m t)} + e^{i(w_0 t - w_m t)}\,\right] - J_2(m)\left[\, e^{i(w_0 t + 2w_m t)} + e^{i(w_0 t - 2w_m t)}\,\right] + \cdots)$$

$$Re(\,E_{PM}\,) = A_0 \times (\, J_0(m)\cos(w_0 t) - J_1(m)\sin(w_0 t + w_m t) - J_1(m)\sin(w_0 t - w_m t) - J_2(m)\cos(w_0 t + 2w_m t) - J_2(m)\cos(w_0 t - 2w_m t) + \cdots$$

The spectrum of the modulated signal contains the frequency of the unmodulated signal and an infinite number of side-bands. They are symmetrical around w_0 at frequencies that are multiples of w_m (fig. 8).

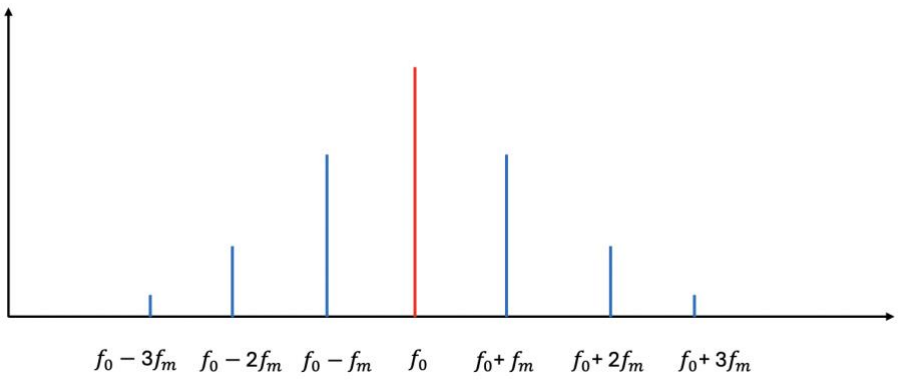

Figure 8: Spectrum of the phase modulated signal, carrier in red and sidebands in blue

Phase modulation creates many sidebands that contains the signal of interest. The number of sidebands that can be detected depends on the modulation index m. The Bessel's function value becomes quickly very small at higher orders when the modulation index is bigger than one (figure 8).

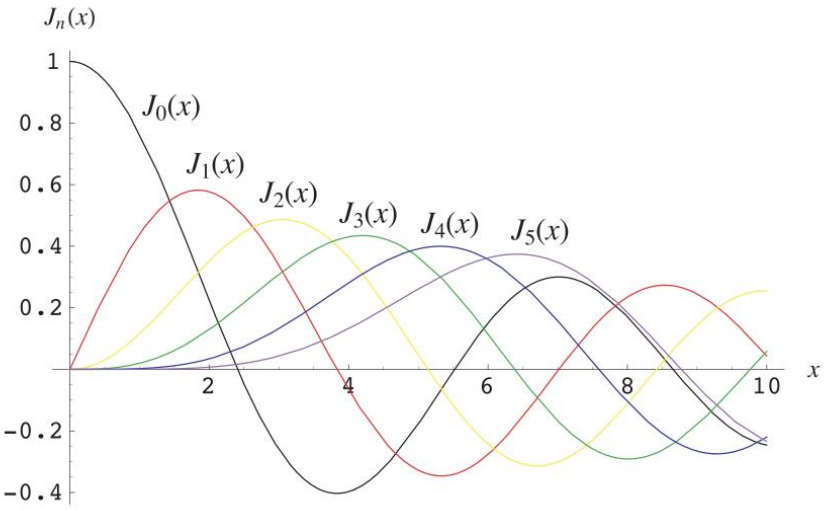

Figure 9: Graph of the Bessel functions of the first kind

2.3. Theory of the beating

Phase modulation cannot be detected directly by photodiodes as they are sensible to amplitude power. A way of measuring phase noise, is to create a beat note between the beam containing the induced phase noise, and a beam of reference. In our setup that will be described in a next part, the beam of reference is the input laser. The beam containing the phase noise is the input beam passing in the other arm to be phase modulated and where phase noise is induced.

The beam of reference can be described with an electric field of:

$$E_{ref} = A_1 \, e^{i(w_0 t + \varphi_0 + \varphi_1)}$$

With A_1 the amplitude, w_0 the reference beam frequency, φ_0 the random initial phase and φ_1 the additional constant phase shift of the optical path difference.

We consider the beam containing the phase noise as:

$$E_{noise} = A_2 \, e^{i(w_0 t + \phi(t) + m \, sin(w_m t) + \varphi_0 + \varphi_2)}$$

With A_2 the amplitude, $\phi(t)$ the phase noise, $m \, sin(w_m t)$ the modulation and φ_2 the additional constant phase shift of the optical path difference.

However, φ_0, φ_1 and φ_2 fluctuates more significantly more slowly than the phase noise $\phi(t)$, we will suppose them constant. The electric field of E_{ref} and E_{noise} can then be written as:

$$E_{ref} = A_1 \, e^{i(w_0 t)}$$

$$E_{noise} = A_2 \, e^{i(w_0 t + \phi(t) + m \, sin(w_m t))}$$

The beating signal is the superposition of E_{ref} and E_{noise} on the photodiode. The power signal detected is given by:

$$P = \left(E_{ref} + E_{noise} \right) \times \left(E_{ref} + E_{noise} \right)^*$$

$$= E_{ref}^2 + E_{noise}^2 + E_{noise}E_{ref}\, e^{i(\phi(t)+m\, sin(w_m t))} + E_{noise}E_{ref}\, e^{-i(\phi(t)+m\, sin(w_m t))}$$

$$= E_{ref}^2 + E_{noise}^2 + 2\, E_{noise}E_{ref} \cos\left(\phi(t) + m\, sin(w_m t)\right)$$

Applying a trigonometric development of the cosines, we obtain:

$$\cos\big(\phi(t) + m\, sin(w_m t)\big) = \cos(m\, sin(w_m t)) \cos\big(\phi(t)\big) - \sin(m\, sin(w_m t))\, sin(\phi(t))$$

By using the real-value variations of the Jacobi-Anger expansion [6]:

$$\cos(x\, sin(\phi)) = J_0(x) + 2J_2(x)\cos(2\phi) + 2J_4(x)\cos(4\phi) + \cdots$$

$$\sin\big(x\, sin(\phi)\big) = 2J_1(x)\sin(\phi) + 2J_3(x)\sin(3\phi) + 2J_5(x)\sin(5\phi) + \cdots$$

By developing until the second order, the expression results in:

$$\cos\big(\phi(t) + m\, sin(w_m t)\big)$$

$$= \cos\big(\phi(t)\big) \times [J_0(m) + 2J_2(m)\cos(2w_m t)] - \sin\big(\phi(t)\big) \times [2J_1(m)\sin(w_m t)]$$

$$= J_0(m)\cos\big(\phi(t)\big) - 2J_1(m)\sin(w_m t)\sin\big(\phi(t)\big) + 2J_2(m)\cos(2w_m t)\cos\big(\phi(t)\big)$$

The Bessel functions of the first kind are given by:

$$J_0(m) = 1 - \left(\frac{m}{2}\right)^2 + \frac{1}{4}\left(\frac{m}{2}\right)^4 - \frac{1}{36}\left(\frac{m}{2}\right)^6 + \cdots$$

$$J_1(m) = \frac{m}{2} - \frac{1}{2}\left(\frac{m}{2}\right)^3 + \frac{1}{12}\left(\frac{m}{2}\right)^5 - \cdots$$

$$J_2(m) = \frac{1}{2}\left(\frac{m}{2}\right)^2 - \frac{1}{6}\left(\frac{m}{2}\right)^4 + \frac{1}{48}\left(\frac{m}{2}\right)^6 - \cdots$$

If we develop the Bessel function until the second order (i.e. supposing m relatively small) we obtain:

$$\cos\big(\phi(t) + m\, sin(w_m t)\big)$$
$$= \left(1 - \left(\frac{m}{2}\right)^2\right) \times \cos\big(\phi(t)\big) - m \times \sin(w_m t)\sin\big(\phi(t)\big)$$
$$+ \left(\frac{m}{2}\right)^2 \times \cos(2w_m t)\cos\big(\phi(t)\big)$$

Note that the same result can be found without using the Bessel functions. If we suppose that the index modulation is small $m \ll 1$ and develop cosine and sin in series around zero until the second order:

$$\cos(m\,sin(w_m t)) \approx 1 - \frac{m^2}{2}\,sin(w_m t)^2$$

$$\sin(m\,sin(w_m t)) \approx m\;sin(w_m t)$$

We obtain the same development of the cosine:

$$\begin{aligned}\cos\big(\phi(t) + m\,sin(w_m t)\big) &= \cos(m\,sin(w_m t))\cos\big(\phi(t)\big) - \sin(m\,sin(w_m t))\,sin(\phi(t)) \\ &\approx \left(1 - \left(\frac{m}{2}\right)^2\right) \times \cos(\,\phi(t)) - m \times \sin(w_m t)\sin\big(\phi(t)\big) \\ &+ \left(\frac{m}{2}\right)^2 \times \cos(2w_m t)\cos(\,\phi(t))\end{aligned}$$

Finally, with either method, if we suppose $m \ll 1$, the complete expression of the power of the beating measured by the photodiode is given by:

$$P = E_{ref}^2 + E_{noise}^2 + 2\,E_{noise}E_{ref}\left(1 - \left(\frac{m}{2}\right)^2\right)\cos(\,\phi(t))$$

$$- 2\,E_{noise}E_{ref}\;m\;\sin(w_m t)\sin\big(\phi(t)\big) + 2\,E_{noise}E_{ref}\left(\frac{m}{2}\right)^2\cos(2w_m t)\cos(\,\phi(t))$$

This resulting power contains a DC part:

$$E_{ref}^2 + E_{noise}^2 + 2\,E_{noise}E_{ref}\left(1 - \left(\frac{m}{2}\right)^2\right)\cos(\,\phi(t))$$

And AC parts that oscillates with the first harmonic f_m of the modulation signal:

$$2\,E_{noise}E_{ref}\;m\;\sin(w_m t)\sin\big(\phi(t)\big)$$

And the second harmonic $2f_m$ of the modulation signal:

$$2\,E_{noise}E_{ref}\left(\frac{m}{2}\right)^2\cos(2w_m t)\cos(\,\phi(t))$$

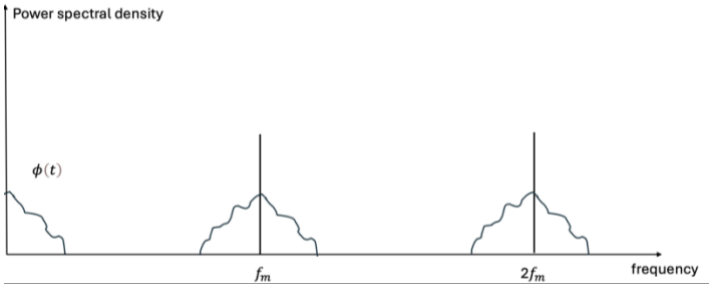

Figure 10: Scheme of the spectrum of the beating signal

By demodulating at the same frequency f_m, we translate back the spectrum. The first harmonic is brought back at 0 Hz and by filtering we can cut the second harmonics and its sidebands so that the signal contains only the phase noise sideband of the first harmonic: $\sin(\phi(t))$ (figure 11). This demodulated signal can then serve as an error signal for a feedback loop as it cancels out at zero and is linear around the working point.

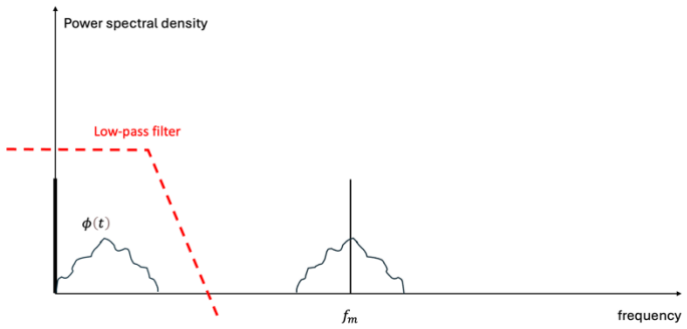

Figure 11: Scheme of the spectrum of the demodulated signal

2.4. Working principal of utilized components

2.4.1. Mirror on a tip / tilt platform

In our project, we require an actuator to modulate in phase the signal and to adjust the phase in the control loop. To achieve this, we can employ a mirror mounted on a tip/tilt platform controlled by piezoelectric elements.

A tilt/tip mirror is designed for laser beam steering in two axes. A mirror is mounted on a tilt/tip stage controlled by a differential piezo drive. Two pairs of low voltage piezoelectric translators push and pull the tilt/tip platform proportionally to the voltage applied (annex 2). However, we don't want to use the piezo in the way it was originally designed. We only want to obtain a translational movement of the mirror in order to shift the phase of the signal.

Moreover, in the setup, the mirror is at a 45° angle to the incident beam and is then collimated and injected into the fiber. Translational movement better maintains alignment with the fiber than a tilt movement. Indeed, a small mirror tilt angle results in greater beam displacement compared to translational displacement, which allows a wider range of piezo amplitude variation before losing the alignment (figure 12 and 13). The alignment is also lost more easily at the collimator when the beam has an angle than when it is only offset from the center where it can be refocused by the collimator lens.

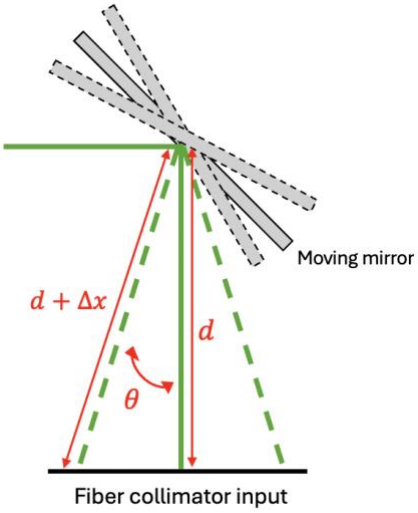

Figure 12: Scheme of a tilt motion

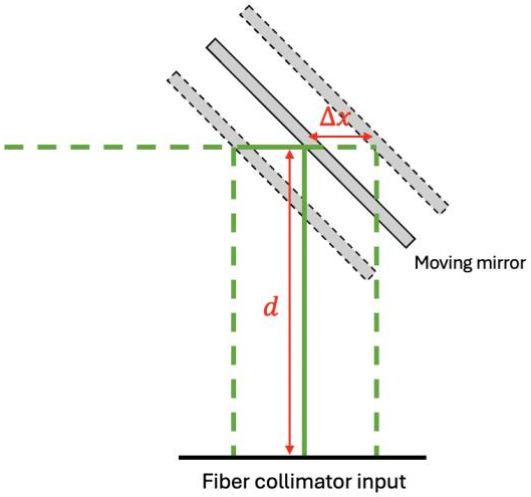

Figure 13: Scheme of a translation motion

The incoming beam comes and is reflected on the mirror with an angle of 45° when the mirror is at its zero position to be then collimated in the fiber. The optical path is not modified and as the length d. When a signal is sent to the mirror it can result in a tilt motion of an angle θ (figure 12) or in a translation motion (figure 13). The optical is then modified by a length Δx.

With the translation motion, we can add $\Delta x = \frac{2}{\sqrt{2}} \times \delta$ to the optical path. Where delta is the expansion length of the piezo actuator. The piezo used in our setup has an expansion range of 15 μm, so we can add a maximum of 21 μm. Since the beam used has a wavelength of 0.532 μm, with a translation motion we have a maximum range of phase shift of 80π. However, in the setup we don't use the entire range as we will lose the alignment, and we finally found that the corrections of the feedback loop induced only a small displacement of the mirror as they were between 0 and 5V.

In practice, achieving translational motion requires applying a specific DC offset and input control value. This differs from the voltage specified in the datasheet (annex 2), which is intended for tilt and tip motion. The tension applied on "CH1" should be the same as on "CH2" and the tension on "CH3" the double of "CH1" and "CH2" so that the potential difference on each piezo is the same.

2.4.2. Fiber stretcher

Another actuator that can be used to introduce a phase shift is the fiber stretcher. It is a device used to tune and modulate the path length of light within an optical fiber, thereby altering the resulting optical delay. This is achieved using voltage-driven piezoelectric ceramics.

In low-frequency linear models, a short section of the fiber is attached to a piezoelectric stack. In high-frequency models, several meters of fiber are wound around a cylindrical piezoelectric element. When a voltage is applied to these piezoelectric elements, they expand, stretching the fiber. The degree of stretching is proportional to the applied voltage: higher voltages result in greater stretching. [8] A low-frequency linear model will be used in the following setup (annex 3). This fiber stretcher as a maximum elongation range of 40 μm. If the entire elongation range is used, it can shift the optical signal up to 150π.

3. Phase noise cancellation experimental setup

3.1. General overview of the setup

The 532nm beam generated by the SHG setup previously described is used as the input of the phase noise cancellation setup. The input beam is splitted by BS1 where 10% of the power is transmitted and measured by the photodiode PD1, and 90% of the power is reflected. This reflected beam is again splitted equally by BS2. One beam is directed toward a « PZT » which correspond to the tilt/tip mirror. It is then injected into long fiber of five meters and a fiber stretcher where phase noise is introduced by the coupling of acoustic noise or by artificially adding phase noise with the fiber stretcher. This noise signal (represented in blue in figure 14) is reflected back by the M6 mirror. The beam goes back to BS2 and is transmitted towards M4 and spiltted again equally on the two photodiodes PD2 and PD3. The other beam transmitted by BS2 does not pass through the fiber is also splitted on PD2 and PD3. This constitutes a beat note between the input signal and the input signal in which phase noise was introduced.

Ultimately, the setup is an interferometer where one arm contains a reference signal and the other contains the modulation and phase noise. Two photodiodes can be used to measure the beating signal to eliminate the common noise of the photodiodes or to leave opportunity for other type of detection. All along this project only one photodiode diode will be used for the measurement.

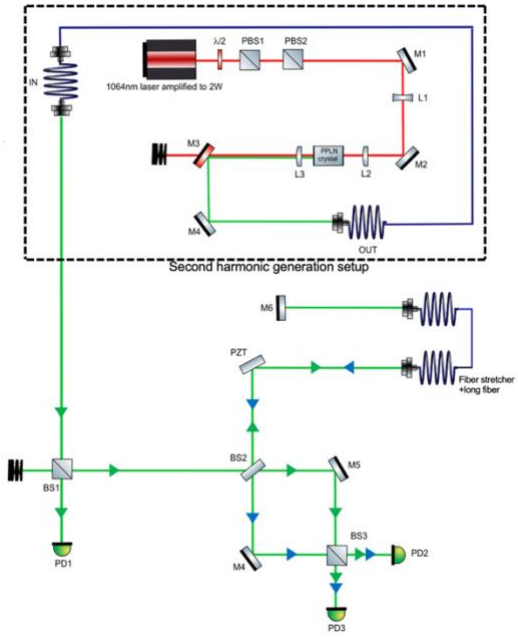

Figure 14: Schematic of the phase noise cancellation setup and SHG setup (circle in black)

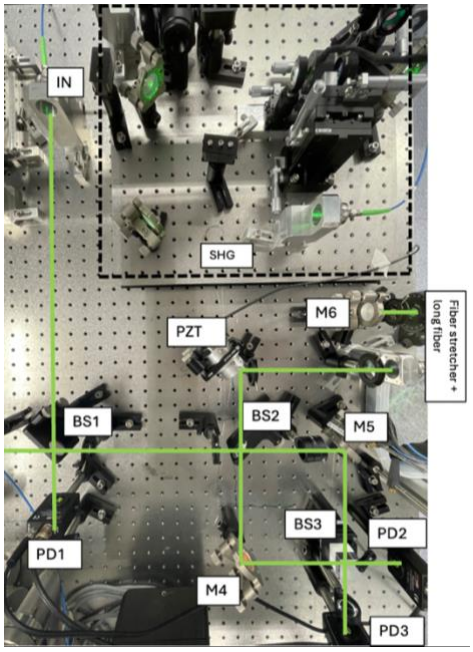

Figure 15: Image of the phase noise cancellation setup and SHG setup (circle in black)

After being measured by the photodiode, the data pass through an ADC, and are visualized using the *dataDisplay* from the *ThinLinc* software which is a tool developed for Virgo to make fast plots in time and frequency domain. The data can also be saved to be further plotted via *MATLAB.* The input control signals for the piezo and the fiber stretcher are sent through a DAC, with commands send with the VPM (Virgo Process Monitoring).

3.2. Modulation and demodulation

We modulate the beating signal to generate sidebands of the phase noise around a carrier. By demodulating, the signal is shifted back, and the phase noise can be measured at lower frequency. The demodulated signal is also used to build the error signal of the feedback loop.

In the setup, modulation is executed at a high frequency (1 kHz) to avoid the laser frequency noise, which decreases inversely with frequency. Ideally, we would prefer to use RF modulation, but no acousto-optic modulator was available for a 532 nm beam. Therefore, we chose the piezo over the fiber stretcher for modulation since the fiber stretcher only operates effectively at frequencies below 500 Hz. At 1 kHz, the piezo offers a good compromise between amplitude and frequency modulation. It can operate at higher frequencies, but we have to decrease the amplitude of the modulation otherwise it enters in resonance.

The demodulation is achieved digitally with VPM, a software line at the modulation frequency is mixed to the modulated signal and filter with a low-pass to extract the signal of interest. The method of demodulation used on VPM is quadrature demodulation. Two mixers are used with different phase offsets to generate an in-phase and a quadrature-phase signal. To obtain the original signal the quadrature output is put to zero and the in-phase output is maximized using a rotating phase operation digitally.

Various modulation configurations (amplitude and frequency) were tested to maximize the phase noise signal. However, the piezoelectric platform limits both the modulation amplitude and frequency due to the risk of resonance that can damage the device. Ultimately, a modulation frequency of 1 kHz and an amplitude of 0.04V were chosen, as this was the highest amplitude that could be applied without causing resonance; at higher frequencies, resonance occurred at lower amplitudes.

The demodulated signal is also filtered at 500 Hz with a low-pass Butterworth filter set on VPM. This filtering cuts the second harmonic of the modulation that is brought back at 1 kHz when demodulating and could dominate the signal of interest which is present at low frequencies.

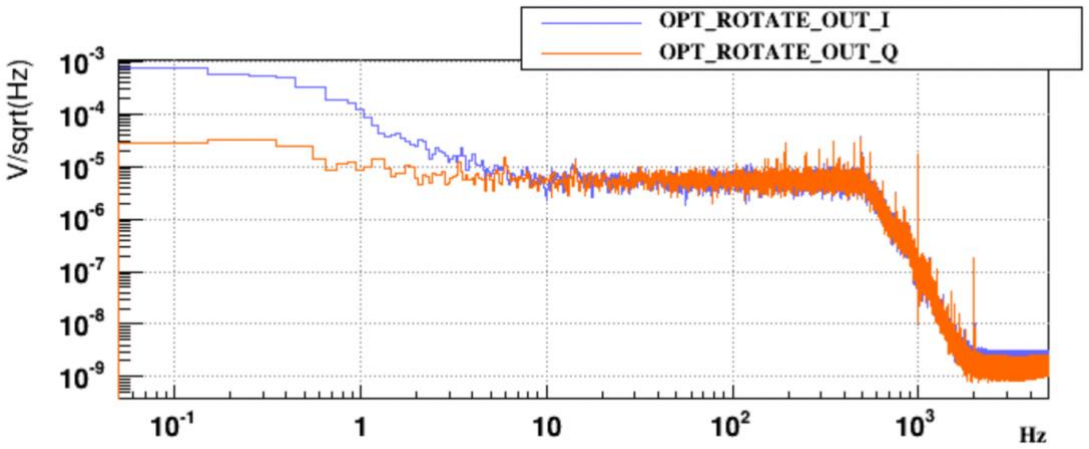

Figure 16: Spectrum of the demodulated signal in-phase, modulated and demodulated at 1 kHz and filtered

In the spectrum of the in phase signal (in blue in figure 16), we can observe the filtering at 500 Hz. From 0 Hz to 10 Hz a signal is present and will be discussed in the next part. Above 10 Hz until 500 Hz the flat area suggest that no signal is present, there is only a sensing noise.

3.3. Beating measurements

The beating measurement is the measurement of the superposition of the signal from the arm of the interferometer containing only the reference (i.e. the laser input) and the other arm containing the modulation, and the phase noise induced. It is measured with the photodiode PD3 (figure 16) sampled with an ADC at 20 kHz therefore according to the Nyquist-Shannon theorem we can measure frequencies until 10 kHz and the average number of FFTs set to ten.

When no signal is applied, the photodiode, which is the PDA10A2 from *Thorlabs*, is characterized by its dark noise (figure 17).

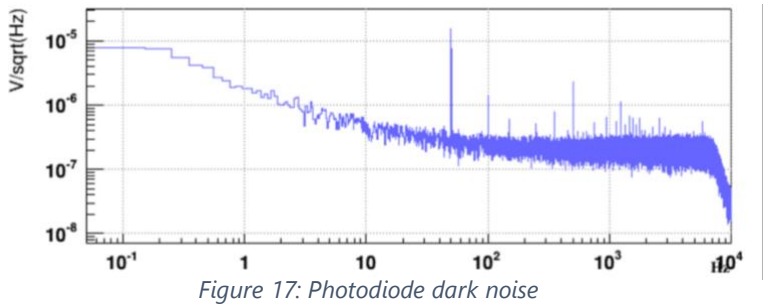

Figure 17: Photodiode dark noise

When no signal is sent, we can see the presence of acquisition noise at low frequencies in the photodiode signal, as well as the 50 Hz of the electronics.

By cutting the beam directly in the setup we can measures the signal coming from each arm and compare it with the beating signal (figure 18).

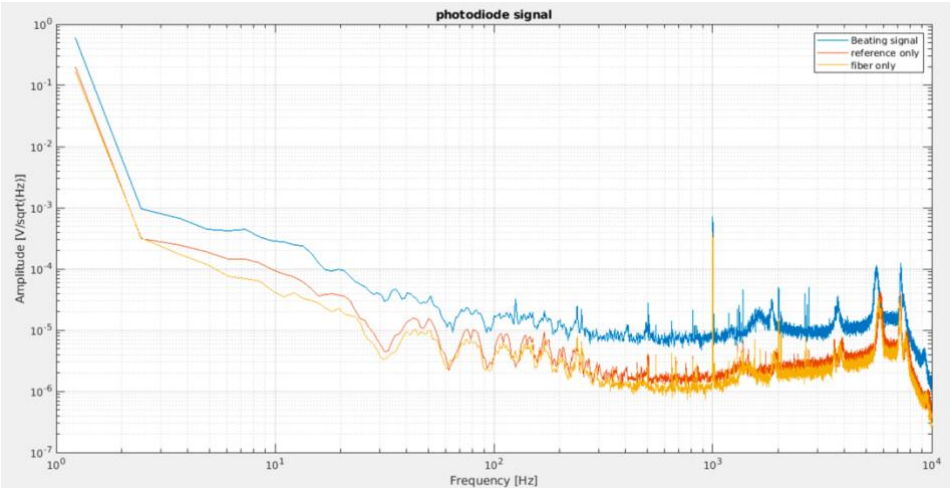

Figure 18: Photodiode signal of the beating and both arms of the interferometer

The signal of the two arms is balanced to obtain approximately the same power (i.e. 0.4V) in each arm, so they are almost superimposed on the FFT signal (in yellow and orange in figure 18). The beating signal has the sum of power of the two arms. The line at 1 kHz corresponds to the modulation line introduced by the piezo which is located in the same arm as the fiber, thus the line is not present in the signal containing only the reference.

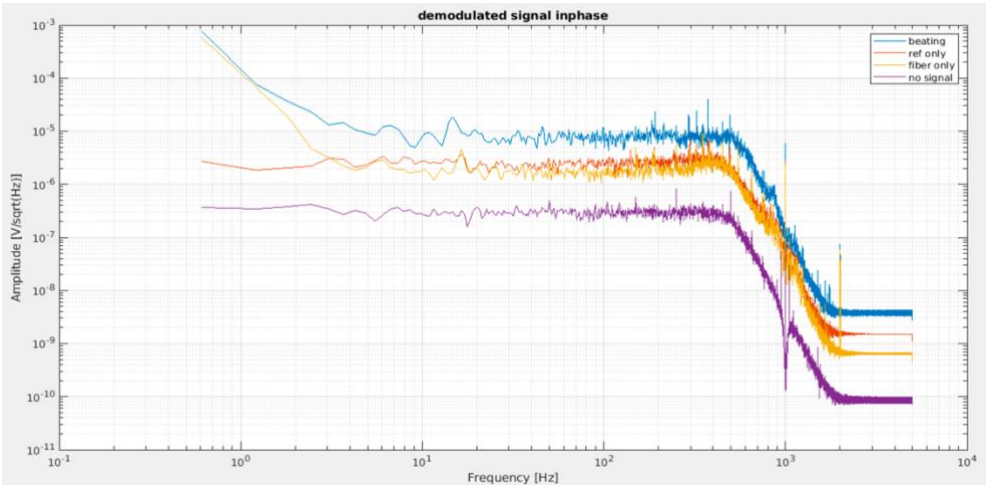

Figure 19: Comparison of the signals of the beating and both arms after demodulation and in phase

After demodulation, a signal is present below 10Hz in the beating signal as well as in the signal of the arm containing the fiber. The signal of the reference only doesn't contain any signal, so we can assume that a phase noise was coupled in the fiber and is present until 10 Hz. Since the phase noise signal is also present in the fiber signal but without the beating, this indicates that in the "fiber only" signal, contains amplitude noise as the photodiode is sensitive to amplitude power. However, the beating signal contains this amplitude noise but also the phase noise that can only be detected by superposing the signal of both arms.

4. Feedback loop

4.1. General overview

The photodiode measures the beating signal that contains the information about the phase difference between the signal of the two arms of the interferometer. In one arm the signal is the local oscillator (the reference signal). In the other, the signal is the input that has passed through the fiber where phase noise was coupled and through an actuator (the piezo platform and/or the fiber stretcher) and is finally superpose on the sensor with the local oscillator.

The addition of the signal of both arms is the beating signal, which is then acquired via an ADC and demodulated, creating a first error signal "Error signal pre". It constitutes the first signal to identify and correct the phase noise. The signal is then normalized relative to the photodiode signal so that it does not depend on the amplitude of the signal measured by the photodiode. A tunable gain is applied to this error signal, the resulting error signal is called "Error signal post".

The controller generates a correction signal digitally with VPM (annex 4) based on the error signal received. The corrector chosen in the setup is defined as:

$$C(p) = \frac{1}{p\,(p + 500)}$$

The integrator is used to correct the signal and the first order with the pole at 500 Hz is used as a low-pass since frequencies above 500 Hz are not used.

The actuator receives the correction signal via a DAC and actuates directly on the optical path. The signal is finally measured by the photodiode to monitor if the phase noise was correctly canceled and loop again (figure 20).

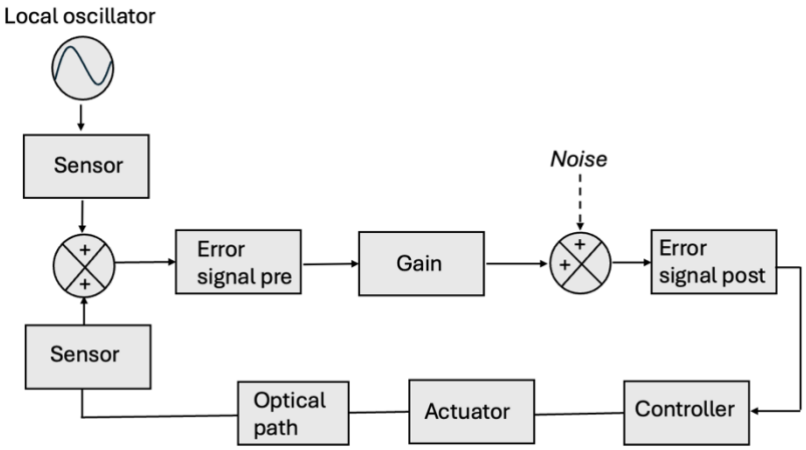

Figure 20: Scheme of the feedback loop

4.2. Open loop transfer function

To better characterize the control loop, we can measure the open loop transfer function. A white noise of a bandwidth of [1 Hz; 50 Hz] is injected after the gain on the error signal (figure 20). The white noise is generated via VPM and is filtered by a bandpass filter to have frequencies of interest. By injecting a noise with a big amplitude relatively to the signal we can consider to be in open loop even if we close the loop and send a gain. The transfer function of the "error signal pre" over the "error signal post" characterize the open loop transfer function (figure 21). The coherence between these two signals is plotted on figure 22.

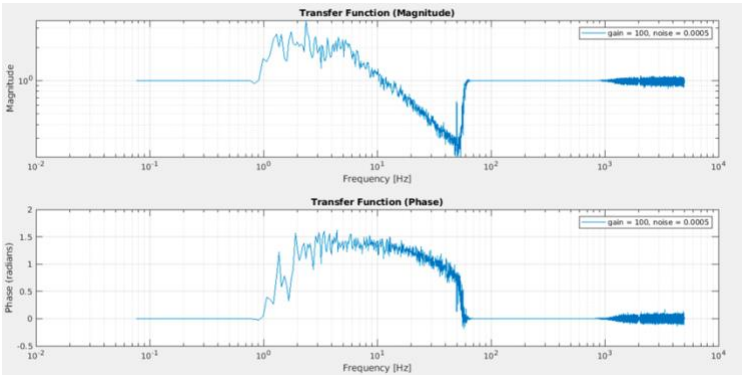

Figure 21: Open loop transfer function

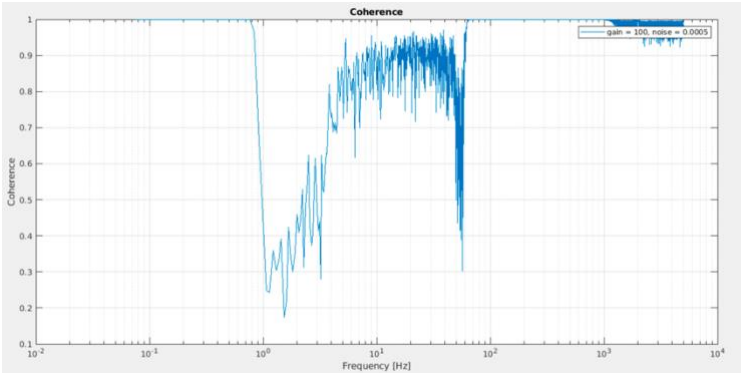

Figure 22: Coherence between "error signal pre" and "error signal post"

The open loop has a unity-gain frequency (UGF) of 11 Hz which is a bit too low to correct acoustic noises that can have frequencies greater than 100 Hz in the fibers used at Virgo. In magnitude the profile of the curve is in one over the frequency which is coherent with the corrector that is a pure integrator. The phase margin is 80° and the phase starts to decrease from 100 Hz, indicating the presence of a delay.

4.3. Results and optimization

The aim of the setup is to cancel the noise that could be observe below 10 Hz on the beating signal demodulated. By using the piezo as an actuator, we were able to close the loop. Depending on the gain applied in the loop we can attenuate the noise more or less (figure 23). To close the loop, we found that the gain should be negative and to fully cancel the noise, it should of -500 or less. Below -1000 the gain is too important and causes a slope below at low frequencies in the curve and pushing again the gain cause the loop to unlock as it became unstable.

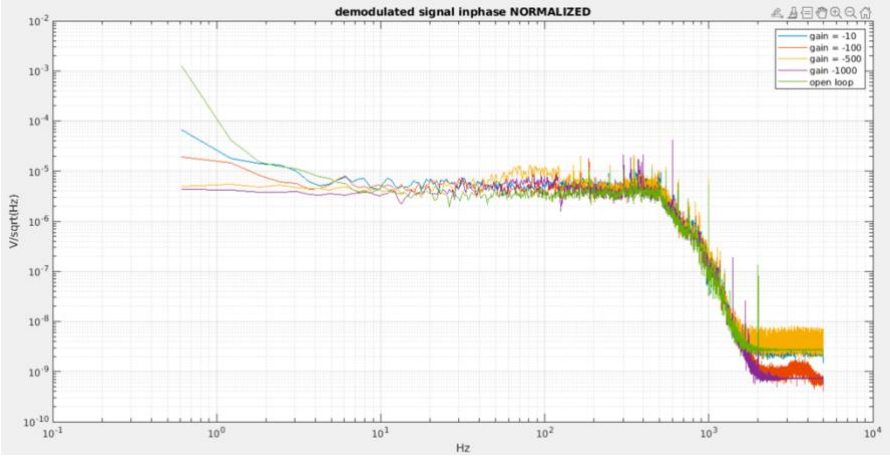

Figure 23: Demodulated signal in phase normalized for different gains and loop closed

For the measurements, the gains were applied one after the other, opening the loop each time before applying them and then closing the loop. As it can be observed in figure 24 where the demodulated signal in phase approaches zero when the loop is closed, and a gain is applied whereas when the loop is open a signal is present and fluctuates. Certain glitches appear on the temporal signal, and we assume they come from the laser's 2W amplifier.

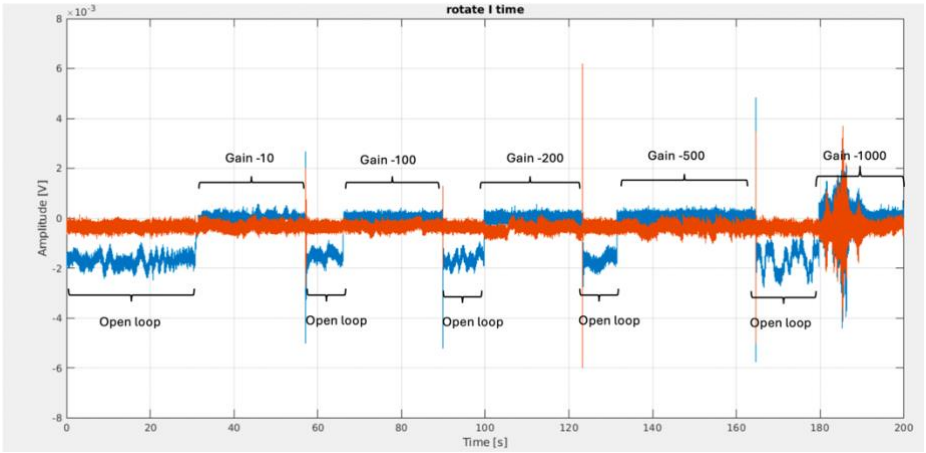

Figure 24: Demodulated signal in phase and in quadrature over time

We also tried using the fiber stretcher as an actuator in the loop instead of the piezo. However, we were unable to close the loop. The correction signal was quickly saturating regardless of the gain applied. A complete characterization of the fiber stretcher and a better understanding of its operation would be necessary to determine if it could be used to close the loop and cancel the noise.

To characterize the attenuation of phase noise, a calibration of the demodulated signal is necessary in order to relate the voltage to the phase shift. However, we were unable to calibrate the demodulated signal, as we were unable to see any saturation coming from the $\sin(\phi(t))$ even when injecting different noises both with the piezo and by touching the fiber directly.

5. Conclusion and perspectives

The purpose of this internship was to develop an optical set-up to cancel optical phase noise induced by an optical fiber with a future perspective of developing a solution for the Auxiliary Laser System of Virgo.

As a first step toward this task, we recommissioned the second harmonic generation setup to generate the green beam needed for the phase noise cancellation setup. A sufficient power was generated to be used as the input of the second setup.

After studying the theory of phase noise and the beating signal. The setup for the phase noise cancellation was built and we were able to measure the signal from both arms of the interferometer and measure the beat note between them. However, the setup could be optimized, especially in terms of alignment and fiber injection, to gain signal and, in particular, increase the power of the signal containing phase noise.

In order to actively cancel the phase noise, a control loop was designed and implemented on VPM. By using the piezo as actuator, the loop could be closed and noise removed. The results are concluding however, the phase noise and its attenuation still remain to be characterized. The correction did not work by using the fiber stretcher as the actuator. The fiber stretcher must therefore be better characterized and understood.

To be really implemented, the correction should be able to reach a unity-gain frequency of 200 Hz which is not achieved with this setup. A setup using RF signals could be considered to achieve this value. Further other detection methods could also be considered using the two photodiodes instead of one as it was done in this project.

ANNEXES

Annex 1 : MATLAB codes for the telescope 24
Annex 2 : S-330 differential tilt/tip platform from PI, working principle 29
Annex 3: Fiber stretcher from IDIL (SER2200204) characteristics 29
Annex 4: Feedback loop code implemented on VPM 30

FIGURES

Figure 1: The optical layout of Advanced Virgo, with dual recycling and Quantum Noise Reduction (Frequency Dependent Squeezing scheme). 4
Figure 2: Schematic of the SHG setup 6
Figure 3: Image of the SHG setup 6
Figure 5: Measurements of the green power generated by the PPLN crystal over the oven's temperature 6
Figure 4: Relation between the periodically poled crystal, its temperature and the wavelength of the input beam 6
Figure 6: Fitted waist size from the different width measurements without the telescope 7
Figure 7: Simulation of the lens's positions of the telescope and beam propagation 7
Figure 8: Spectrum of the phase modulated signal, carrier in red and sidebands in blue 9
Figure 9: Graph of the Bessel functions of the first kind 10
Figure 10: Scheme of the spectrum of the beating signal 12
Figure 11: Scheme of the spectrum of the demodulated signal 13
Figure 12: Scheme of a tilt motion 14
Figure 13: Scheme of a translation motion 14
Figure 14: Schematic of the phase noise cancellation setup and SHG setup (circle in black) 16
Figure 15: Image of the phase noise cancellation setup and SHG setup (circle in black) 16
Figure 16: Spectrum of the demodulated signal in-phase, modulated and demodulated at 1 kHz and filtered 17
Figure 17: Photodiode dark noise 18
Figure 18: Photodiode signal of the beating and both arms of the interferometer 18
Figure 19: Comparison of the signals of the beating and both arms after demodulation and in phase 19
Figure 20: Scheme of the feedback loop 20
Figure 21: Open loop transfer function 20
Figure 22: Coherence between "error signal pre" and "error signal post" 20
Figure 23: Demodulated signal in phase normalized for different gains and loop closed 21
Figure 24: Demodulated signal in phase and in quadrature over time 21

Annex 1 : MATLAB codes for the telescope

```
clear all; close all;
% Waist of incident beam
% z0 =-10.0;      % Waist Location
% w0= 290e-6;
% lambda=1064e-9;
% npt=1000;
%syntaxe : comp = [Propagation, focal lenght of the lens, Propagation ...]
z0 =-1.6;      % Waist Location
w0= 800e-6;
lambda=1064e-9;
npt=1000;

% %%%%%%%%%%%%%%%%%%%%%%%%%%%%%%%%
% %%%%%% not moving lens %%%%%%%%
% %%%%%%%%%%%%%%%%%%%%%%%%%%%%%%%%

f1=-0.143;
f2=0.035;
f3=0.035;
 % %offset = 0;
 comp=[0.44,f1,0.137,f2,0.13,f3,0.5];
% %
 [H_w1,H_p1,H_Rc,mmmrad,sw0,zw0] = GaussRay(comp,npt,lambda,w0,z0,1);
%
 ztot=sum(comp(1:2:length(comp)));
 fprintf('ztot = %.4g mm', ztot*1000);
 fprintf('\nztot-wpos = %.4g m \n \n', (ztot-zw0));

% % % %%%%%%%%%%%%%%%%%%%%%%%%%%%%%
% % % %%%%%% moving lens %%%%%%%%%%
% % % %%%%%%%%%%%%%%%%%%%%%%%%%%%%%
  f1=-0.143;
  f2=0.035;
  f3=0.035;

  Vect_offset = linspace(0.06,0.2,10); %m
%
  Vect_sw0 = zeros(1,length(Vect_offset));
  Vect_zw0 = zeros(1,length(Vect_offset));
  for i=1:length(Vect_offset)
%
  offset= Vect_offset(i);
%
  comp=[0.44, f1, 0.137, f2, offset, f3, 0.5];
%
% %[H_w1,H_p1,H_Rc,mmmrad,sw0,zw0] = GaussRay(comp,npt,lambda,w0,z0,1);
%
[H_w1,H_p1,H_Rc,mmmrad,sw0,zw0] = GaussRay(comp,npt,lambda,w0,z0,1)
%
  ztot=sum(comp(1:2:length(comp)));
  fprintf('ztot = %.4g mm', ztot*1000);
  fprintf('\nztot-wpos = %.4g m', (ztot-zw0));
%
  Vect_sw0(i) =sw0;
 Vect_zw0(i) =zw0;
 pause;
  end
```

```
%
 figure
 [AX,H1,H2] = plotyy(Vect_offset,Vect_sw0*1e6,Vect_offset,Vect_zw0*1e3);
 grid on ;
 set(get(AX(1),'Ylabel'),'String','waist size (um)');
 set(get(AX(2),'Ylabel'),'String','waist position (mm)') ;
```

Functions used in this code:

GaussRay function:

```
function [we,gph,curvature,mm_mrad,sw0,zw0,w,Zout] = GaussRay(comp,npt,lambda,w0,z0,Plots)
% GAUSSRAY  Gaussian ray tracing (one-dimensional, TEM00)
%   function [we,gph] = gaussray(comp,npt,lambda,w0,z0)
% Traces beam diameter and Gouy phase of a Gaussian beam over the
% propagation distance. Shows also the geometrical beam construction.
% Spaces and lenses are defined in the component vector. Units are meters.
%
%  comp    Component vector, containing free space propagation and lenses
%          Structure : [L1,f1,L2,f2,...,Ln], where Li are the propagation
%          distances, and fi are the lens focal lengths. So the vector
%          can have 1, 3, 5, ... elements.
%  npt     Number of points to plot
%  lambda  wavelength
%  w0      input beam waist radius
%  z0      input beam waist position (with respect to the beginning
%          of the first propagation).
%  we      beam radius after total beam path
%  gph     integrated Gouy phase after total beam path (in deg.)
% Example:
%   GaussRay([0.4,0.5,1,0.2,0.3],100,1.064e-6,0.001,-1)
% Traces a beam with lenses of 500 and 200 mm over a total beam path of 1.7m.
%
%                                   H. Heitmann 11.06.2005

we = 0;
gph = 0;

if mod(length(comp),2)==0
  disp('Component vector must begin and end with a propagation space');
  return
end
for i=1:2:length(comp)
  if comp(i)<0
    disp('All distances must be positive');
    return
  end
end

z_tot = sum(comp(1:2:length(comp)));

% Calculate points
for n = 1:npt
  z = z_tot*n/npt;
  [w(n),phi(n),Rc(n),pp,aa,mat,q_fin] = GaussMat(comp,lambda,w0,z0,z);
  a(n) = aa(1); p(n) = pp(1);
end

%Waist size and position for the last propagation
zw0=  z_tot - real(q_fin) ;
sw0= sqrt(imag(q_fin)*lambda/pi);
```

```
%fprintf('Waist size and position for the last propagation: \n w0_size: %.4g um, \n w0_position: %.4g mm
\n',sw0*1e6,zw0*1e3);

%////////////Ri ch
  R_p = mat*[1;0];
  R_a = mat*[0;1];
  mm_mm = R_p(1);
  mrad_mm = R_p(2);
  mm_mrad = R_a(1);
  mrad_mrad = R_a(2);
% fprintf('\n Richard Results (pure shifts/tilts at input):\n %.2g mm/mm,  %.2g mm/mrd,  %.2g mrd/mm,  %.2g mrd/mrd
\n\n',...
%        mm_mm,...  %   mm/mm
%        mm_mrad,...  %   mm/mrad
%        mrad_mm,...  % mrad/mm
%        mrad_mrad...  % mrad/mrad
%        );
%////////////Rich
% Eliminate Gouy phase jumps at lens positions
for i=2:2:length(comp)
  z_lens = sum(comp(1:2:i-1));
  [tmp,phi1,tmp,mat] = GaussMat(comp(1:i-1),lambda,w0,z0,z_lens);
  [tmp,phi2,tmp,mat] = GaussMat(comp(1:i),lambda,w0,z0,z_lens);
  n = floor(npt*(z_lens/z_tot-1e-7));
  phi = phi - (1:npt>n)*(phi2-phi1);
end
% Center tilted geometrical ray on center of first lens
%a = a - comp(1)*p;
a = a - a(1);
% Normalize geometrical rays to plot
a = a*max(w)/max(abs(a))/2;
p = p*max(w)/max(abs(p))/2;
zx = (1:npt)/npt*z_tot;
if(Plots)
   % Plot results

   ax(1) = subplot(311);
   plot(zx,1000*w,'b',zx,-1000*w,'b',zx,1000*a,'k--',zx,1000*p,'r-.',zx,0*zx,'k:');
   ylabel('Beam diameter [mm]');
   text = sprintf('[%g] %g ',comp);
   title(['Telescope: ' text])

   % Draw lens positions
   hold on;
   zd = z_tot/10000;
   nz = 10; % Space between lens lines
   for i=2:2:length(comp)
     z = sum(comp(1:2:i));
     plot([z-5*zd,z-5*zd],-1200*max(w)*[-1,1],'k')
     plot([z+5*zd,z+5*zd],-1200*max(w)*[-1,1],'k')
   end
   hold off
   axis('tight')
   ax(3) = subplot(313);
   %plot(zx,phi/90,'r');
   plot(zx,phi,'r');
   xlabel('Beam path [m]'); ylabel('Gouy phase [deg]')
   text = sprintf('w0=%gmm, z0X=%gm, lambda=%gnm',1000*w0,z0,1e9*lambda);
   title([text])
   grid; axis('tight')
   % subplot(313)
   % plot((1:npt)/npt*z_tot,Rc,'g');
   linkaxes(ax,'x');

   ax(2) = subplot(312);
```

```
   plot(zx,1000*w,'b',zx,-1000*w,'b',zx,1000*a,'k--',zx,1000*p,'r-.',zx,0*zx,'k:');
   ylabel('Beam diameter [mm]');
   text = sprintf('[%g] %g ',comp);
   title(['Centered on the waist: ' text])
   axis([0.5 0.7 -2 2]);

end
Zout=zx;
gph = phi(npt);
we  = w(npt);
curvature = Rc(npt);

dz = z_tot/npt;
%fprintf('Beam waist and Gouy phase at end of plot: %.4g um, %.1f deg.\n \n',...
 %       1e6*we,gph);
%fprintf('Geometrical telescope enlargement (pure shifts/tilts at input):\n %.4g mm/mm,  %.4g mm/mrd,  %.4g mrd/mm,
%.4g mrd/mrd \n\n',...
%       p(npt)/p(1),...  %   mm/mm
%       a(npt)/((a(2)-a(1))/dz),...  %   mm/mrad
%       (p(npt)-p(npt-1))/dz/p(1),...  % mrad/mm
%       (a(npt)-a(npt-1))/(a(2)-a(1))...  % mrad/mrad
%       );

%=========================================================

function [w,phi,Rc,p,a,mat,q] = GaussMat(comp,lambda,w0,z0,z)
% Calculates the propagation matrix of a Gaussian beam having waist
% w0 at position z0, through a series of elements specified in the
% component vector comp (to begin with a propagation space), from 0 to z.
% Returns beam radius, Gouy phase (not glued), beam curvature.
% Optionally returns also the geometrical evolution of an incoming parallel
% and angular ray (p,a).
zR = pi*w0^2/lambda;
q0 = sqrt(-1)*zR-z0;

mat = [[1 0];[0 1]];
z_i = 0;
for i=1:length(comp)
  if mod(i,2)==1  % space
    if sum(comp(1:2:i))>z break ; end
    mat = [[1 comp(i)];[0 1]] * mat;
    z_i = sum(comp(1:2:i));
  else          % lens
    mat = [[1 0];[-1/comp(i) 1]] * mat;
  end
end
mat = [[1 z-z_i];[0 1]] * mat; % treat remaining space

q   = (q0*mat(1,1)+mat(1,2))/(q0*mat(2,1)+mat(2,2));
w   = sqrt(abs(q)^2*lambda/pi/imag(q));
phi = atan(real(q)/imag(q))*180/pi;

if nargout>3
  p = mat*[1;0];
  a = mat*[0;1];
end
Rc  = abs(q)^2/real(q);  %arbitrary change

%Rc  = q^2/real(q);
```

GaussMat function :

```
function [q] = GaussMat(comp,lambda,w0,z0,z)
% Calculates the propagation matrix of a Gaussian beam having waist
% w0 at position z0, through a series of elements specified in the
```

```
% component vector comp (to begin with a propagation space), from 0 to z.
% Returns beam radius, Gouy phase (not glued), beam curvature.
% Optionally returns also the geometrical evolution of an incoming parallel
% and angular ray (p,a).
zR = pi*w0^2/lambda;
q0 = sqrt(-1)*zR-z0;

mat = [[1 0];[0 1]];
z_i = 0;
for i=1:length(comp)
  if mod(i,2)==1  % space
    if sum(comp(1:2:i))>z break ; end
    mat = [[1 comp(i)];[0 1]] * mat;
    z_i = sum(comp(1:2:i));
  else          % lens
    mat = [[1 0];[-1/comp(i) 1]] * mat;
  end
end
mat = [[1 z-z_i];[0 1]] * mat; % treat remaining space

q   = (q0*mat(1,1)+mat(1,2))/(q0*mat(2,1)+mat(2,2));
w   = sqrt(abs(q)^2*lambda/pi/imag(q));
phi = atan(real(q)/imag(q))*180/pi;

if nargout>3
  p = mat*[1;0];
  a = mat*[0;1];
endfunction [q] = GaussMat(comp,lambda,w0,z0,z)
% Calculates the propagation matrix of a Gaussian beam having waist
% w0 at position z0, through a series of elements specified in the
% component vector comp (to begin with a propagation space), from 0 to z.
% Returns beam radius, Gouy phase (not glued), beam curvature.
% Optionally returns also the geometrical evolution of an incoming parallel
% and angular ray (p,a).
zR = pi*w0^2/lambda;
q0 = sqrt(-1)*zR-z0;

mat = [[1 0];[0 1]];
z_i = 0;
for i=1:length(comp)
  if mod(i,2)==1  % space
    if sum(comp(1:2:i))>z break ; end
    mat = [[1 comp(i)];[0 1]] * mat;
    z_i = sum(comp(1:2:i));
  else          % lens
    mat = [[1 0];[-1/comp(i) 1]] * mat;
  end
end
mat = [[1 z-z_i];[0 1]] * mat; % treat remaining space

q   = (q0*mat(1,1)+mat(1,2))/(q0*mat(2,1)+mat(2,2));
w   = sqrt(abs(q)^2*lambda/pi/imag(q));
phi = atan(real(q)/imag(q))*180/pi;

if nargout>3
  p = mat*[1;0];
  a = mat*[0;1];
end
```

Annex 2 : S-330 differential tilt/tip platform from PI, working principle

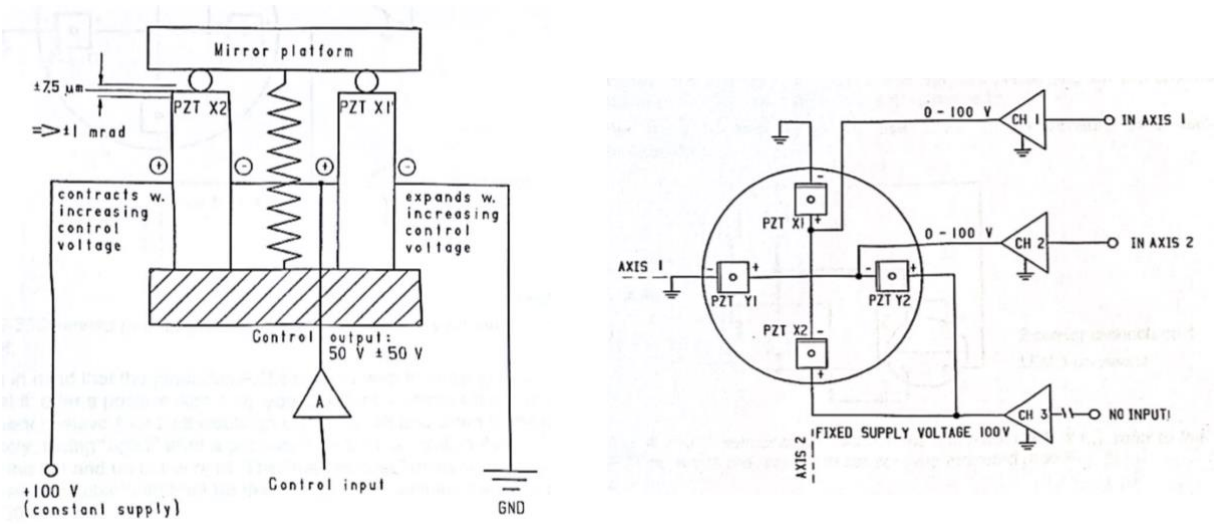

Annex 3: Fiber stretcher from IDIL (SER2200204) characteristics

Fiber stretcher	PM 460
Connectors (IN/OUT)	FC/APC PM - FC/APC PM
Pigtails length (IN/OUT)	L= 0,5m (+/-0,02)
Buffer	900 µm
Insertion loss	< 0,3 dB
Elongation range 40 µm	0-150 V
Phase shift	0,3 µm/V +/- 0,05

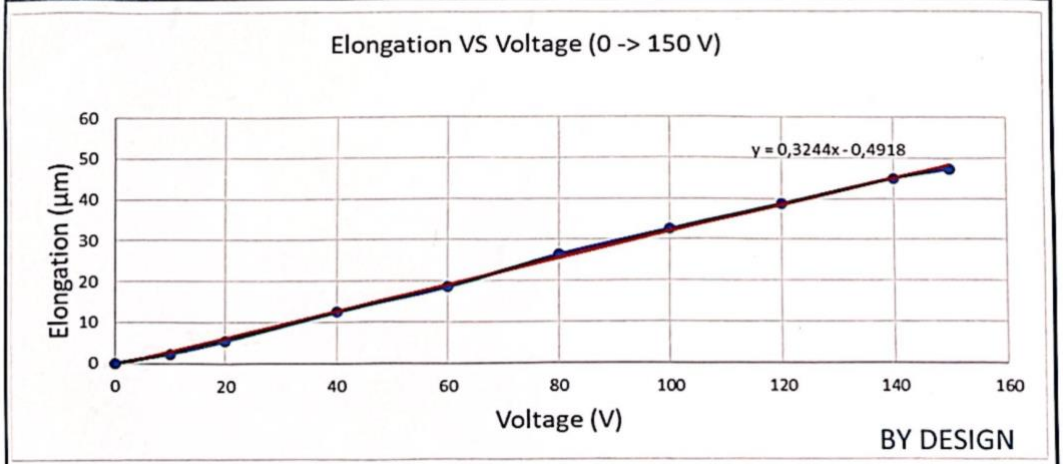

Annex 4: Feedback loop code implemented on VPM

```
#Beating signal
ACL_ADC_CH   "Beating"              ""              1       LOOP_FREQ    "Ampli_out"                  0
        1               "DAQ_FILTER_10KHZ" #

#PZT lines
ACL_SINELINE_CH  "PZT_modulation"  "V"     LOOP_FREQ    1000    0.
#ACL_SINEWAVE_CH  "PZT_noise"  "V"  1.   LOOP_FREQ   0.5   33.5    0.   0.
#ACL_SUM_CH "PZT_SUM"     "V"    1       0.1 "PZT_modulation"  0       "PZT_noise"

#Demodulation
ACL_DEMOD   "PZT_DEMOD"   1   LOOP_FREQ   "Beating"   "PZT_modulation"   "PZT_demod_flt"   0.0   "mag|phi"

#Demodulation with constant phase applied
#ACL_CONST_CH   PZT_DEMOD_phi0    "rad"0.0  LOOP_FREQ          1.9
#ACL_CONST_CH   "PZT_DEMOD_phi0"     ""   1   LOOP_FREQ   1PI/4
#ACL_DEMOD   "PZT_DEMOD"   1   LOOP_FREQ   "Beating"   "PZT_modulation"   "NONE"   -1PI/4   "Beating"
ACL_ROTATE_CH   "ROTATE_OUT"   1   "PZT_DEMOD_I"   "PZT_DEMOD_Q"  2.7 "mag"

#Normalization of the demodulated signal inphase
ACL_OP_CH   "ROTATE_OUT_NORM"   "V"   "ROTATE_OUT_I"   "/"   "Beating"   0

#Error signal
ACL_CONST_CH   "GAIN_PHASE"   "V"   1.0   LOOP_FREQ   0
ACL_RELAY_CH   "PHASE_ON""V"     LOOP_FREQ    0.001   0.001   0
ACL_OP_CH    "Ampli_ERR"   "V"    "prod" "ROTATE_OUT_NORM"  "GAIN_PHASE" "PHASE_ON"
ACL_SUM_CH "Ampli_ERR_TOT"   "V"   1   1 "Ampli_ERR"   0 "Sensing_NOISE"

#Definition of the loop filter
ACL_FILTER_SET    "integrator"    1   1   10   4
ACL_FILTER_POLES   "integrator"    0   0
ACL_FILTER_POLES   "integrator"    500   0

#Correction signal
ACL_FILTER_CH         "Ampli_CORR"  "au"    1       LOOP_FREQ    "Ampli_ERR_TOT"              1       "integrator"
ACL_FILTER_CH_RESET_CND            "Ampli_CORR"  "PHASE_ON"

#PZT control signal
ACL_CONST_CH   "DOUBLE"   "V"   1.0   LOOP_FREQ   2
ACL_CONST_CH   "OFFSET"   "V"   1.0   LOOP_FREQ   0.04
ACL_SUM_CH   "PZT_SUM"     "V"    1       0.04 "PZT_modulation"   0.0  "OFFSET"   1.0 "Ampli_CORR"   0.0
"Sensing_sin_noise"
#ACL_SUM_CH   "PZT_SUM_NOISE"   "V"   1   1   "PZT_SUM"   1 "Ampli_CORR"
ACL_CLIP_CH   "PZT_SUM_CLIP"   "PZT_SUM"   -5   5
ACL_OP_CH    "PZT_SUM_DOUBLE"   "V"    "prod" "PZT_SUM_CLIP"  "DOUBLE"
ACL_CLIP_CH   "PZT_SUM_DOUBLE_CLIP"   "PZT_SUM_DOUBLE"   -5   5

#Fiber stretcher control signal
ACL_CONST_CH   "OFFSET_FIBER"   "V"   1.0   LOOP_FREQ   5
ACL_SUM_CH   "FIBER_SUM"   "V"    1   1.0 "OFFSET_FIBER"   #1.0 "Ampli_CORR"   #0 "Sensing_sin_noise"
ACL_CLIP_CH   "FIBER_SUM_CLIP"   "FIBER_SUM"   0   10
```

[1] Virgo-gw. URL : https://www.virgo-gw.eu/science/detector/

[2] Wilfried Jan, Internship report SHG, VIR-0436A-14

[3] RP Photonics, Frequency doubling. URL : https://www.rp-photonics.com/frequency_doubling.html

[4] RP Photonics, Phase Noise. URL: https://www.virgo-gw.eu/science/detector/optical-layout/

[5] Fritz Riehle, Frequency Standards Basics and Applications, Wieley-VCH, ISBN 3-527-40230-6

[6] Andrew Gray, George Ballard Mathews, A treatise on Bessel Functions and Their Applications to Physics, Macmillan, 1895, Chap III p18

[7] PI. PZ 107E User Manual S-330 Tip/Tilt Platform, 09/09/2003

[8] IDIL. URL : https://www.idil-fibres-optiques.com/product/fiber-stretcher-2/

Résumé

L'objet de ce stage était la suppression du bruit de phase optique dans une fibre. Pour accomplir cet objectif, un montage permettant la génération d'un faisceau vert a été mis en place dans un premier temps. Ce faisceau est ensuite utilisé comme entrée du second montage optique permettant la suppression du bruit de phase. Après avoir étudié la théorie du bruit de phase et les signaux de battement, le second montage a été construit. Nous avons pu mesurer le signal des deux bras de l'interféromètre et leur battement. Pour annuler activement le bruit, une boucle de contrôle a été conçue et implémentée. En utilisant le piézo comme actionneur, la boucle a pu être fermée et le bruit supprimé. Cependant, des améliorations et optimisations sont nécessaires, notamment sur l'étirement de fibre et la calibration du signal d'erreur. Afin d'améliorer la correction, une autre méthode de détection peut être envisagée ainsi que l'utilisation de signaux RF.

Mots clés: bruit de phase optique, interféromètre, boucle de contrôle, piezo, fiber stretcher

Summary

The purpose of this internship was the suppression of optical phase noise in a fiber. To achieve this objective, a setup for generating a green beam was implemented first. This beam is then used as the input for the second optical setup, which allows the suppression of phase noise. After studying the theory of phase noise and beating signals, the second setup was constructed. We were able to measure the signal from both arms of the interferometer and their beating. To actively cancel the noise, a control loop was designed and implemented. By using the piezo as an actuator, the loop could be closed, and the noise suppressed. However, improvements and optimizations are necessary, especially regarding the fiber stretcher and the calibration of the error signal. To enhance the correction, another detection method can be considered, as well as the use of RF signals.

Keywords: optical phase noise, interferometer, control loop, piezo, fiber stretcher

ENSI CAEN

ÉCOLE PUBLIQUE D'INGÉNIEURS
CENTRE DE RECHERCHE

Ecole Publique d'Ingénieurs en 3 ans

6 boulevard Maréchal Juin, CS 45053
14050 CAEN cedex 04

ministère éducation nationale enseignement supérieur recherche

Normandie Université

Cti Commission des titres d'ingénieur

cdefi Conférence des Directeurs des Écoles Françaises d'Ingénieurs

European Accreditation of Engineering Programmes EUR-ACE®

CONFÉRENCE DES GRANDES ÉCOLES